MID-LATITUDE COMPOSITION OF MARS FROM THERMAL AND EPITHERMAL NEUTRONS.
T.H. Prettyman,[1] W.C. Feldman,[1] R.C. Elphic,[1] W.V. Boynton,[2] D.L. Bish,[1] D.T. Vaniman,[1] H.O. Funsten,[1] D.J. Lawrence,[1] S. Maurice,[3] G.W. McKinney,[1] K.R. Moore,[1] and R.L. Tokar[1] [1]Los Alamos National Laboratory, Los Alamos, New Mexico. [2]Lunar and Planetary Laboratory, University of Arizona, Tucson. [3]Observatoire, Midi-Pyrenees (Toulouse, France).

Introduction: Epithermal neutron data acquired by Mars Odyssey have been analyzed to determine global maps of water-equivalent hydrogen abundance [1]. By assuming that hydrogen was distributed uniformly with depth within the surface, a map of minimum water abundance was obtained. The addition of thermal neutrons to this analysis could provide information needed to determine water stratigraphy. For example, thermal and epithermal neutrons have been used together to determine the depth and abundance of water-equivalent hydrogen of a buried layer in the south polar region [2,3].

Because the emission of thermal neutrons from the Martian surface is sensitive to absorption by elements other than hydrogen, analysis of stratigraphy requires that the abundance of these elements be known. For example, recently published studies of the south polar region [2,3] assumed that the Mars Pathfinder mean soil composition is representative of the regional soil composition. This assumption is partially motivated by the fact that Mars appears to have a well-mixed global dust cover and that the Pathfinder soil composition is representative of the mean composition of the Martian surface [4].

In this study, we have analyzed thermal and epithermal neutron data measured by the neutron spectrometer subsystem of the gamma ray spectrometer to determine the spatial distribution of the composition of elements other than hydrogen. We have restricted our analysis to mid-latitude regions for which we have corrected the neutron counting data for variations in atmospheric thickness.

Composition or Stratigraphy? The emission of epithermal neutrons from Mars is sensitive to hydrogen abundance and stratigraphy to within about a meter of the surface. Thermal neutrons are also sensitive to hydrogen abundance and stratigraphy; however, because the cross section for thermal neutron capture is large at thermal energies, they are also sensitive to the composition of elements such as Fe and Cl, as well as rare earth elements, Gd and Sm, which have large absorption cross sections. Consequently, thermal and epithermal neutrons cannot be used to independently determine water abundance and stratigraphy when the composition of major elements other than hydrogen is unknown.

To illustrate this point and to gain some insight into whether composition varies in the mid-latitudes, we analyzed measured neutron count rates for selected regions in Tharsis. Epithermal and thermal neutron count rate maps are shown in Figs. 1 and 2, respectively, for the western hemisphere mid-latitudes (±60° latitude and -180° to 0° east longitude). These 2° quasi-equal-area maps were constructed using data acquired from the beginning of mapping in late February 2002 (L_S=346°) through January 2003 (L_S=131°). The maps have been corrected for variations in atmospheric mass to enable comparison to neutron count rates calculated for an atmospheric mass of 16 g/cm^2 [5]. The thermal and epithermal count rate model that we used for this study takes into account the ballistic trajectories of the neutrons and their half life, the velocity and orbit of the spacecraft, and the response function of the neutron spectrometer. The model was calibrated using data acquired near the north pole when the seasonal CO_2 frost was thickest [1].

Three regions of interest are shown on the thermal neutron map: Region A contains the Tharsis volcanic shields, including Olympus Mons; Region B contains Solis Planum; and Region C contains the highlands surrounding Solis Planum and extends into Valles Marineris. A scatter plot of thermal and epithermal count rates measured within these regions is shown in Fig. 3. Also shown in Fig. 3 are calculated count rates for three different surface materials mixed with variable amounts of water-equivalent hydrogen. The materials are: Mars Pathfinder mean soil (labeled "Soil" in Fig. 3) and soil-free rock (labeled "Andesite" in Fig. 3), and shergotty (labeled "Basalt" in Fig. 3) [4,6].

The red curves in Fig. 3 show the variation of count rate with water abundance for each of the three materials for the case in which the distribution of water is uniform with depth. Count rates are shown for water abundances ranging from 0.5% to 100% for the soil composition and from 0.5% to 10% for basalt and andesite. The epithermal neutron count rate decreases with increasing water abundance and is relatively insensitive to other changes in composition. The thermal neutron count rate, as indicated by the red curves is strongly sensitive to material type (soil, andesite, or basalt) due to variations in major absorbers.

The macroscopic absorption cross section for thermal neutrons was determined to be 11.6 capture units (1 c.u. = 10^{-3} cm^2/g) for the soil, 9.1 c.u. for andesite, and 7.9 c.u. for the basalt. Changes in Cl and Fe abundance between the materials account primarily for the differences in the absorption cross section and the

simulated count rates. However, Cl, which has an absorption cross section that is 13 times that of Fe, dominates the variation in the macroscopic absorption cross section. We used a Cl composition of 0.55% by weight for the soil, 0.32% for the andesite, and 0.01% for the basalt.

The red curves in Fig. 3 give an upper bound on thermal neutron count rates for a given material type (soil, andesite, or basalt). It is possible to achieve lower count rates by varying the stratigraphy of hydrogen. We have modeled cases in which a water-rich layer is buried beneath relatively dry material. Such cases are indicated in Fig. 3 for the soil composition by dashed lines and symbols. One set of cases, corresponding to 100% water buried beneath different amounts of soil containing 1% water, is labeled with the depth of the buried water-rich layer in g/cm^2. Note that in the limit, as depth of the water rich layer increases, the count rate approaches that of the dry upper layer.

The measured thermal count rates for the volcanic shield region (Region A, shown as red symbols in Fig. 3) exceed the maximum count rate that can be achieved for Mars Pathfinder soil, as indicated by the red curve labeled "Soil." The count rates are more consistent with the basalt composition. The thermal neutron count rates in Solis Planum (Region B, shown as green symbols in Fig. 3) are also more consistent with basalt than with soil. The thermal neutron count rates for the highlands surrounding Solis Planum (Region C, shown as yellow symbols in Fig. 3) are lower but still exceed the maximum count rate expected for Pathfinder soil. Thermal neutron count rates for the western hemisphere mid-latitudes (shown as blue symbols in Fig. 3) extend below the maximum count rate for Pathfinder soil. Consequently, some regions with composition consistent with the soil exist in the western hemisphere between latitudes ±40°. However, the regions examined in Tharsis are not consistent with this composition, probably due to relatively low Cl abundance associated with volcanic materials. Note that small variations in Cl abundance can significantly affect the thermal neutron output because the cross section for Cl is large. It is not possible to determine from thermal and epithermal neutrons alone whether observed differences in thermal neutron count rate are due to changes in hydrogen stratigraphy or changes in the abundance of thermal neutron absorbers.

Maps of Neutron Cross Sections: Feldman et al. [7] developed and demonstrated methods to determine bulk neutron transport properties of planetary surfaces from orbital thermal and epithermal counting data. Using these methods, we have developed maps of neutron scattering and absorption cross sections for

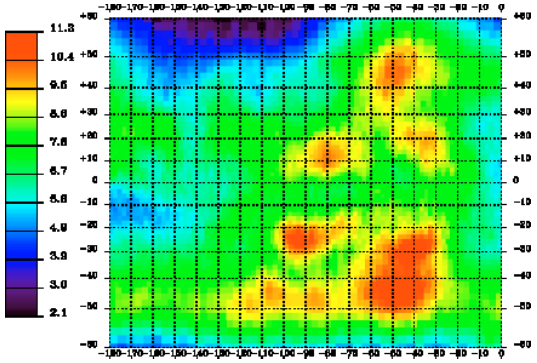

Fig. 1. Map of epithermal neutron count rates (counts/s) in the western hemisphere mid-latitudes (±60° latitude; -180° to 0° east longitude).

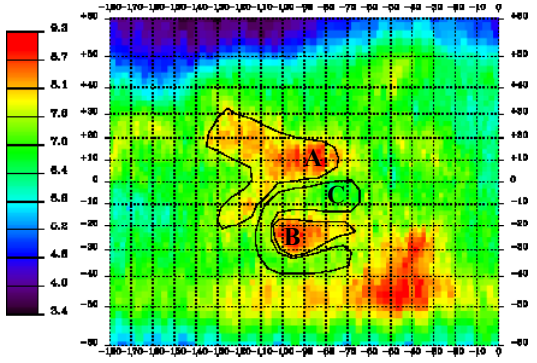

Fig. 2. Map of thermal neutron count rates (counts/s) in the western hemisphere mid-latitudes (±60° latitude; -180° to 0° east longitude). Some regions of interest are shown.

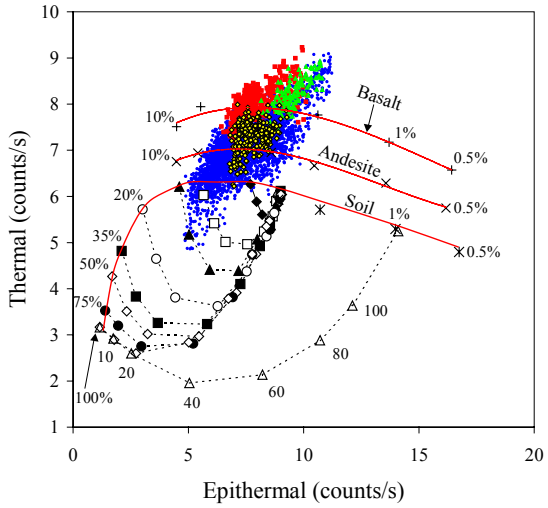

Fig. 3. Simulated and measured thermal neutron count rates are shown. The measured count rates correspond the regions delineated in Fig. 2. Counting data from Region A is shown as red symbols; data from Region B is shown as green symbols; data from Region C is shown as yellow symbols; and data from the western hemisphere between ±40° latitude is shown as blue symbols. A description of the simulated count rates is given in the text.

the Martian mid-latitudes. The analysis assumes that there is no variation in composition (hydrogen or otherwise) with depth. Epithermal neutrons are used to determine $\xi\Sigma_s$, the product of the mean fractional energy loss per elastic collision (ξ) and the macroscopic scattering cross section (Σ_s). The ratio of epithermal to thermal neutrons is used to determine $\Delta=\Sigma_a/\xi\Sigma_s$, where Σ_a is the macroscopic absorption cross section for thermal neutrons.

In order to determine the relationship between the measured count rates and the neutron transport parameters, we simulated thermal and epithermal count rates for 60 different compositions, including soil, basalt and andesite with variable amounts of hydrogen and Cl. The materials were selected to span the count rates observed by the Mars Odyssey neutron spectrometer at mid-latitudes. For each composition, we calculated the transport parameters Σ_a, ξ, Σ_s, $\xi\Sigma_s$, and Δ.

Using data from all 60 simulated compositions, we found the following relationship between $\xi\Sigma_s$ and the epithermal neutron count rate:

$$\xi\Sigma_s = 1.5966 C_{epi}^{-1.6091}. \quad (1)$$

The correlation coefficient of the regression was found to be $R^2=0.9988$. We found the following relationship between Δ and the ratio of the epithermal to thermal count rate:

$$\Delta = 0.2146(C_{epi}/C_{therm}) - 0.0753, \quad (2)$$

The correlation coefficient for the regression was found to be $R^2=0.9987$. Using Eqs. 1 and 2, we calculated mid-latitude maps of $\xi\Sigma_s$ and Δ, which are shown in Figs. 4 and 5, respectively. A map of Σ_a obtained by multiplying $\xi\Sigma_s$ by Δ is shown in Fig. 6.

Note that the map of $\xi\Sigma_s$ is very similar to the map of minimum water abundance developed by Feldman et al. [1]. The mean fraction energy loss and scattering cross section are strongly dependent on hydrogen abundance and are relatively insensitive to other elements. The map of Σ_a is correlated with the map of $\xi\Sigma_s$, which may be partially explained by the fact that thermal neutron capture by hydrogen is non-negligible. The microscopic absorption cross section is 0.33 barns. The correlation coefficient was found to be $R^2=0.67$.

Using the map of minimum water abundance reported by Feldman et al. [1], we determined the contribution of hydrogen to the macroscopic absorption cross section of Martian materials at mid-latitudes. We then subtracted the hydrogen macroscopic cross section from our map of Σ_a to determine a map of the absorption cross section of all elements other than hydrogen. The resulting map, shown in Fig. 7, is similar to the map of the total absorption cross section shown in Fig. 6. The correlation between Σ_a and $\xi\Sigma_s$ remains following the subtraction of the contribution from hydrogen ($R^2=0.55$).

The correlation of the absorption cross section for elements other than H with $\xi\Sigma_s$, which is directly related to the abundance of water-equivalent hydrogen, may indicate past processing of surface materials by water. The highest values in the absorption cross section occur northward of the dichotomy boundary in Acidalia Planitia and Utopia Planitia. These are lowlands in which standing water may have existed on or near the surface, possibly resulting in the formation of Cl-salts.

Conclusions: In this study, we analyzed thermal and epithermal neutron data to determine whether the composition of elements other than hydrogen varied significantly in the Martian mid-latitudes. We mapped the macroscopic absorption and scattering cross sections in the mid latitudes assuming there was no variation of composition with depth. The absorption cross section for elements other than hydrogen was found to be generally correlated with minimum water abundance. This suggests that the absorption cross section is sensitive to aqueous alteration of surface materials. The highest values in the absorption cross section occur northward of the dichotomy boundary in Acidalia Planitia and Utopia Planitia. These are lowlands in which standing water may have existed on or near the surface, possibly resulting in the formation of Cl-salts.

Comparison of measured count rates from three regions in Tharsis with simulated count rates for different materials shows that Tharsis materials are more consistent with basalt than with the mean Pathfinder soil composition. Lower Cl in basaltic materials may result in elevated thermal neutron count rates in the volcanic shield region and Solis Planum.

Capture gamma rays from Cl and Fe are detected by the gamma ray spectrometer. Maps of these elements with sufficient spatial resolution will be developed once sufficient counting precision is achieved. The abundance of Cl and Fe and the stratigraphy of water-equivalent hydrogen will eventually be determined through simultaneous analysis of both the neutron and gamma ray data. The neutron transport parameters we have mapped can be used to estimate the thermal neutron number density in the surface [8], enabling gamma ray counting data to be converted accurately into estimates of elemental abundance.

References: [1] Feldman W.C., et al. (2003) this proceedings, #3218. [2] Boynton, W.V., et al. (2002) *Science 297*, 81-85. [3] Tokar, R.L., et al. (2002) *Geophys. Res., Lett. 29*, doi:10.1029/2002GL015691. [4] Wanke H., et al. (2001) *Space Science Reviews 96*, 317-330. [5] Prettyman T.H. et al. (2003) *LPSC 34*, #1950. [6] Laul J.C., et al. (1986) *Geochim. Cosmochim. Acta 50*, 909-926. [7] Feldman W.C. et al. (2000) *JGR 105*, 20,347-20,363. [8] Lawrence D.J. et al. (2002) *JGR* 107, 10.1029/2001JE001530.

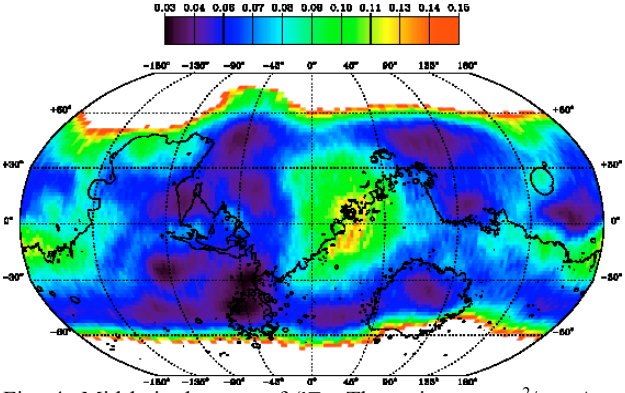

Fig. 4. Mid-latitude map of $\xi\Sigma_s$. The units are cm^2/g. A contour of topography at 0 km elevation is superimposed on the map.

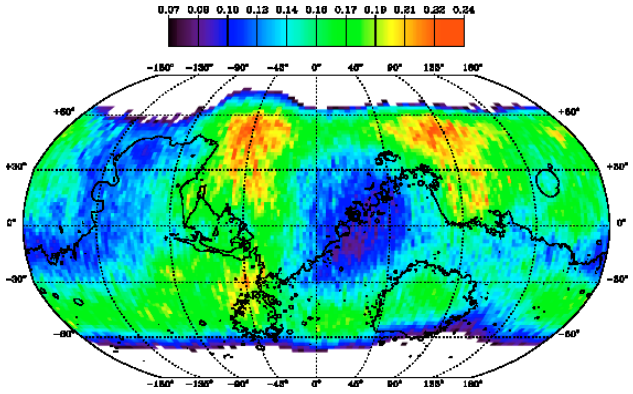

Fig. 5. Mid-latitude map of Δ. A contour of topography at 0 km elevation is superimposed on the map.

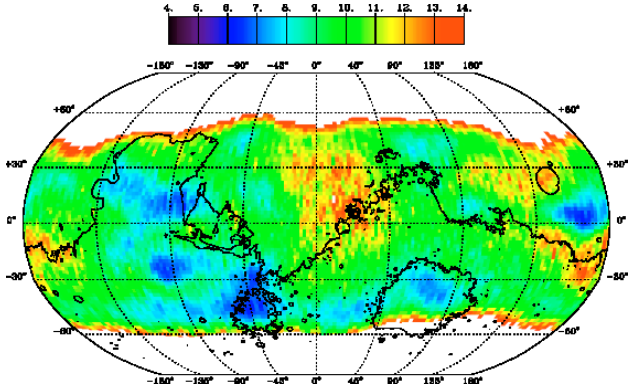

Fig. 6. Mid-latitude map of the total macroscopic absorption cross section, Σ_a. The units are 10^{-3} cm^2/g. A contour of topography at 0 km elevation is superimposed on the map.

Figure 7 (below). Mid-latitude map of the partial macroscopic absorption cross section (the contribution from hydrogen is removed). The units are 10^{-3} cm^2/g. A contour of topography at 0 km elevation is superimposed on the map.